*Research Article*
Hittite Journal of Science and Engineering, 2023, 10 (3) 201–209
ISSN NUMBER: 2148–4171
DOI: 10.17350/HJSE19030000308

# Electrochemical Dopamine Detection Using Palladium/ Carbon Nano Onion Hybrids

**Hasan Huseyin Ipekci**[1,2]
[1]Necmettin Erbakan University, Department of Metallurgical and Materials Engineering, Konya, Türkiye
[2]Necmettin Erbakan University, BITAM, Konya, Türkiye

## ABSTRACT

In the given study, palladium-decorated carbon nano-onion nanostructures (Pd/CNO) were used as an electrochemical catalyst for detecting dopamine (DA). The physicochemical properties of the Pd/$SO_3$H/CNO-based catalysts were studied by transmission electron microscopy (TEM), scanning electron microscopy (SEM), X-ray diffraction (XRD), and X-ray photoelectron spectroscopy (XPS) methods. Pd/$SO_3$H/CNO inks were dropped cast on a glassy carbon electrode (GCE) to prepare the electrochemical DA sensors. The sensor performance was performed using cyclic voltammetry (CV), differential pulse voltammetry (DPV), and electrochemical impedance spectroscopy (EIS). The electroanalytical results indicated a LOD value of 2.44 µM and the linear range of the sensors were found to be between 10 and 400 µM DA. The enhanced electrocatalytic activity toward DA is attributed to the high active surface area, conductivity of CNO and the high electrocatalytic property of Pd. The results suggest that Pd/$SO_3$H/CNO nanostructures can be used to detect electrochemical DA sensors with high selectivity, sensitivity, and low LOD.

***Article History:***
*Received: 2023/01/13*
*Accepted: 2023/07/05*
*Online: 2023/09/30*

***Correspondence to**: Hasan Huseyin Ipekci, Necmettin Erbakan University, Metallurgical and Materials Engineering, 42090, Konya, TÜRKİYE*
*E-Mail: hhipekci@erbakan.edu.tr, hsnpkc@gmail.com;*

***This article has been checked for similarity.***



**Keywords:**
Carbon nano-onion; Palladium; Electrochemical sensor; Dopamine; Differential pulse voltammetry

## INTRODUCTION

Carbon and its allotropes have gained tremendous attention in electrochemical sensing applications owing to their chemical stability, high electrocatalytic activity, biocompatibility, conductivity, low cost, and large surface areas [1, 2]. So far, carbon-related materials including carbon black, carbon nanotubes (CNT), graphene, graphene oxide, amorphous carbon, and carbon nano-onion (CNO) have been used as the sensing materials for different molecules. Among these, CNO shows great potential for electrochemical applications due to having the structure of multiple concentric shells of fullerenes, quasi-spherical and polyhedral-shaped layers. The distance between the polyhedral-shaped layers ranges from 3 to 50 nm [3]. CNOs demonstrate unique chemical and physical properties, such as good biocompatibility, low toxicity, high electronic conductivity, and thermal stability. Besides, the tolerability of the surface functional groups renders the CNO structures highly dispersible in aqueous solutions. CNO and its derivatives have been used in different electrochemical applications such as energy storage [4], bioimaging [5], magnetic storage media [6], fuel cell electrodes [7], and sensing and biomedical applications [8]. For the case of electrochemical sensing applications, various reports have shown the applicability of CNO-based materials against the detection of different molecules such as glucose [9, 10], dopamine [11, 12] cysteine; methionine [13] epinephrine, and norepinephrine [12], phenoxy herbicides [14].

Although pristine carbon allotropes show electrochemical activity to some extent, the pristine structure does not yield a high electrochemical activity compared to metal and metal oxide-based electrocatalysts. One of the most effective methods to achieve enhanced electrochemical performance in carbon-based catalysts is the decoration of the carbon surface with metal nanoparticles (MNPs). Some MNPs reported in the literature are Ag [15, 16], Pt [17-19], Pd [20, 21], and Au [22]. The incorporation of MNPs in the catalyst structures boosts the electrochemical activity of the electrochemical sensors significantly. MNPs anchored on the carbon surface facilitate electron transfer and can act as electron transfer mediators, which leads to enhanced electrochemical performance. Pd is one of the most exploited noble metals to decorate the carbon surface for enhanced electrochemical activity in different electrochemi-

**Cite as:**
*Ipekci H I, "Electrochemical Dopamine Detection Using Palladium/Carbon Nano Onion Hybrids". Hittite Journal of Science and Engineering 2023;10(3): 201-209. doi:10.17350/hjse19030000308*

cal applications such as energy storage [23], medicine [24], oxygen reduction [25], sensing [26] and waste treatment [27].

Dopamine (DA) is a bioactive molecule that plays vital roles in the human body and is a neurotransmitter for the messaging cognitive function and diseases in the central and peripheral nervous system. Hence, the DA level in the blood is the indicator of various diseases, and its detection with high selectivity and sensitivity is of great importance. While a low DA level in the human brain can cause schizophrenia, addiction [28], depression [29], and diseases such as Parkinson's [30] and Alzheimer's[31], a high level of DA may cause hypertension, drug addiction, and heart failure [32]. The level of DA has been determined using conventional methods including colorimetric [33], fluorescence [34], chromatography [35] and electrochemical methods. Those conventional methods, however, pose disadvantages such as complicated sample pre-treatments, time-consuming testing procedures, and the requirement of expensive equipment. Therefore, electrochemical sensors are of great importance because of the advantages of easy operation and low cost, fast response, high stability and selectivity [36]. Breczko et al. detected DA using CNO/PDDA (poly(diallyl dimethylammonium chloride) nanocomposite in a range of $5x10^{-5}$ and $4x10^{-3}$ mol/L [11]. A screen-printed electrode was constructed with CNO and graphite mixture ink and the sensor detected dopamine in the linear range from 10 μM to 99.9 μM, and the lowest detection concentration was 0.92 μM [37]. Carbon nano-onions and their derivatives have been exploited to detect DA electrochemically [12, 38].

The given work depicts the preparation of Pd/$SO_3H$/CNO nanocomposites to develop electrochemical DA sensors with high sensitivity and selectivity. Pd nanoparticles were precipitated on the $SO_3H$-modified CNO surface using a facile chemical precipitation method. The decoration of CNO surface with $SO_3H$ groups prevent the agglomeration of the nanoparticles due to acting as a nucleation agent. In the given work, Pd-decorated $SO_3H$/CNO nanohybrids were exploited to construct electrochemical DA sensors, for the first time in the literature. The physicochemical properties of the catalysts were studied using TEM, SEM, XPS, XRD, Raman, and FTIR methods. CV and DPV were used to determine the electrochemical performance of Pd/$SO_3H$/CNO against DA for sensitivity, selectivity, storage stability, repeatability, and applicability of the sensors in real samples.

## EXPERIMENTAL

### Chemicals

$CuCl_2$*$2H_2O$ (99%) and $CaC_2$ (75%) were purchased from Merck an $NH_3$*$H_2O$ (28%-30%), $NaBH_4$ (96%), $K_2PdCl_4$, chloroform, Nafion (5 wt.%), and dopamine were purchased from Sigma-Aldrich. The interferents molecules (hydrogen peroxide, glucose, uric acid, and ascorbic acid) were obtained from Sigma. No additional treatment was applied to the chemicals.

### Synthesis of CNO, $SO_3H$/CNO, and Pd/$SO_3H$/CNO

Carbon nano-onions were prepared based on a study reported by Han et al. [39]. Briefly; $CuCl_2$*$2H_2O$ (0.059 mol) and $CaC_2$ (0.05 mol) were placed in a 30 ml stainless steel autoclave and left in an oven which was hold at 600°C for 10 h. The obtained product was washed with $NH_3$*$H_2O$ and chloroform to remove the copper residues. After that, the obtained carbon phase was rigorously washed with deionized water and ethanol and left for drying in a vacuum oven overnight. The surface of the obtained CNO powder was modified with $SO_3H$ groups to enhance the distribution of Pd nanoparticles. It should be emphasized that $SO_3H$ groups on the carbon surface act as nucleation agents for Pd NPs, which results in an enhancement in the homogeneous distribution of MNPs on the surface [40, 41]. Within this aim, the CNO surface was furnished with $SO_3H$ groups using a method explained as follows. 1 g of sulfonic acid (99%, Sigma) was dissolved in a solution containing NaOH (2 wt.%), then 0.4 g of sodium nitrate was introduced. After homogenization, the obtained solution was added slowly into 10 ml ultrapure water at ice temperature (0°C) and kept stirring for 30 min. After that, the solution was slowly added to the 30 mL CNO/DI water suspension in an ice bath and stirred for another 5 h. The modified CNO structures were centrifuged, washed with DI, and dried in a vacuum oven. Pd nanoparticles were anchored on $SO_3H$/CNO surfaces using a method reported in a previous study [42]. Briefly, a certain amount of $SO_3H$/CNO was dispersed in DI containing $K_2PdCl_4$ at 55°C for 12 h. Then, freshly prepared $NaBH_4$ was slowly added to the solution dropwise and Pd nanoparticles were allowed to precipitate on the nanocarbon surface. Solid phase was removed from the liquid phase by centrifugation and dried.

### Characterization of CNO, $SO_3H$/CNO and Pd/$SO_3H$/CNO

X-ray diffraction (XRD) was used for phase identification by using Rigaku Ultims-IV equipped with Cu Kα (λ=0.15406 nm) radiation. The diffraction pattern was scanned over 20°–90° 2θ, at a scanning speed of 1° 2θ/min. The average size and distribution of Pd nanoparticles deposited on carbon nano-onion structures were determined using transmission electron microscopy (TEM, FEI @ 200kV). Morphology, surface properties, and elemental analysis (EDS) of nanostructures were determined by scanning electron microscopy (Zeiss Gemini SEM 500,

SEM). Additionally, the bond structures and the oxidation states of the nanostructures were determined by X-ray photoelectron spectroscopy (XPS, PHI 5000 VersaProbe).

### Preparation of the sensor, electrochemical analyses

The catalyst inks were composed by mixing a certain amount of obtained powder, Nafion solution (5% v/v, 30 µl), DI water (0.6 ml), and ethanol (0.4 ml). To homogenize the ink, an ultrasonic bath and probe were used. Before the application of the ink slurries on the GC surface (3mm in diameter), the electrode surface was polished with alumina slurry. The surface of the GC was covered with 5 µl of the ink and left for drying. To form a permselective membrane on the sensor surface and improve the stability of the sensors, Nafion solution (0.05 wt.%) was dropped on the Pd/$SO_3$H/CNO -modified GC surface. Electrochemical measurements were performed using an Emstat3 Blue (Netherlands) potentiostat. A Pt plate was used as the counter electrode and the reference electrode was Ag/AgCl. In the electrochemical experiments, 0.1 M PBS buffer was used as the electrolyte. Determination of DA was carried out by CV and DPV methods. EIS analysis was performed using a PalmSens 4 potentiostat in an electrolyte containing 5 mM $K_3[Fe(CN)_6]$/ $K_4[Fe(CN)_6]$ in 0.1 M KCl. The DPV analysis was carried out between -0.4 and 0.8 V with a pulse amplitude of 25 mV, a pulse width of 70 ms, and a scan rate of 25 mV/s. Frequency range of 82500 and 0.05 Hz was chosen as the EIS parameters and the data were recorded with a pulse amplitude of 5mV by using PalmSens4.

## RESULT AND DISCUSSION

### Characterization of the CNO and Pd/$SO_3$H/CNO

Representative TEM images of the as-synthesized CNO samples are given in Fig. 1. The images indicated the formation of the carbon structure after the heat treatment of $CuCl_2$*$2H_2O$ and $CaC_2$. The high-magnification TEM image (Fig. 1b) showed carbon fringes and when the obtained results were compared with the literature, it can be suggested that CNO nanoparticles were successfully synthesized. The TEM images of the Pd-modified $SO_3$H/CNO structures are also given in Fig. 1c-d. The images suggest that Pd nanoparticles were evenly distributed on $SO_3$H/CNO surface without any severe agglomeration. As discussed earlier, the modification of the CNO surface with $SO_3$H functionalities improved the Pd distribution, preventing the agglomeration of the MNPs. Additionally, small Pd nanoparticles (< 10 nm) were anchored on the carbon surface.

XRD was used to determine the phase analysis and the recorded XRD diffractograms are displayed in Fig. 2a. The XRD peaks appearing at about the 2θ values of 40.3°, 46.6 °, 68.2 °, and 82.3° are responsible for the planes of (111), (200), (220), and (311), respectively in the face-centered cubic Pd nanoparticles. In addition to metallic Pd, the oxide form

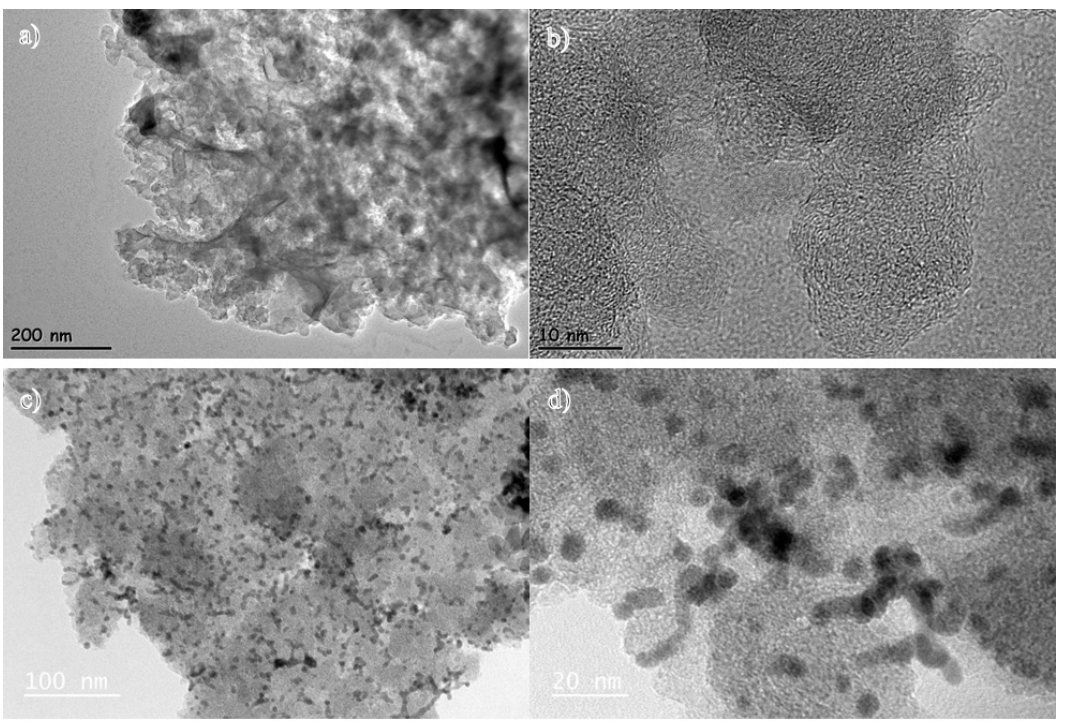


**Figure 1.** TEM images of CNO (a-b) and Pd/$SO_3$H/CNO (c-d) at different magnifications.

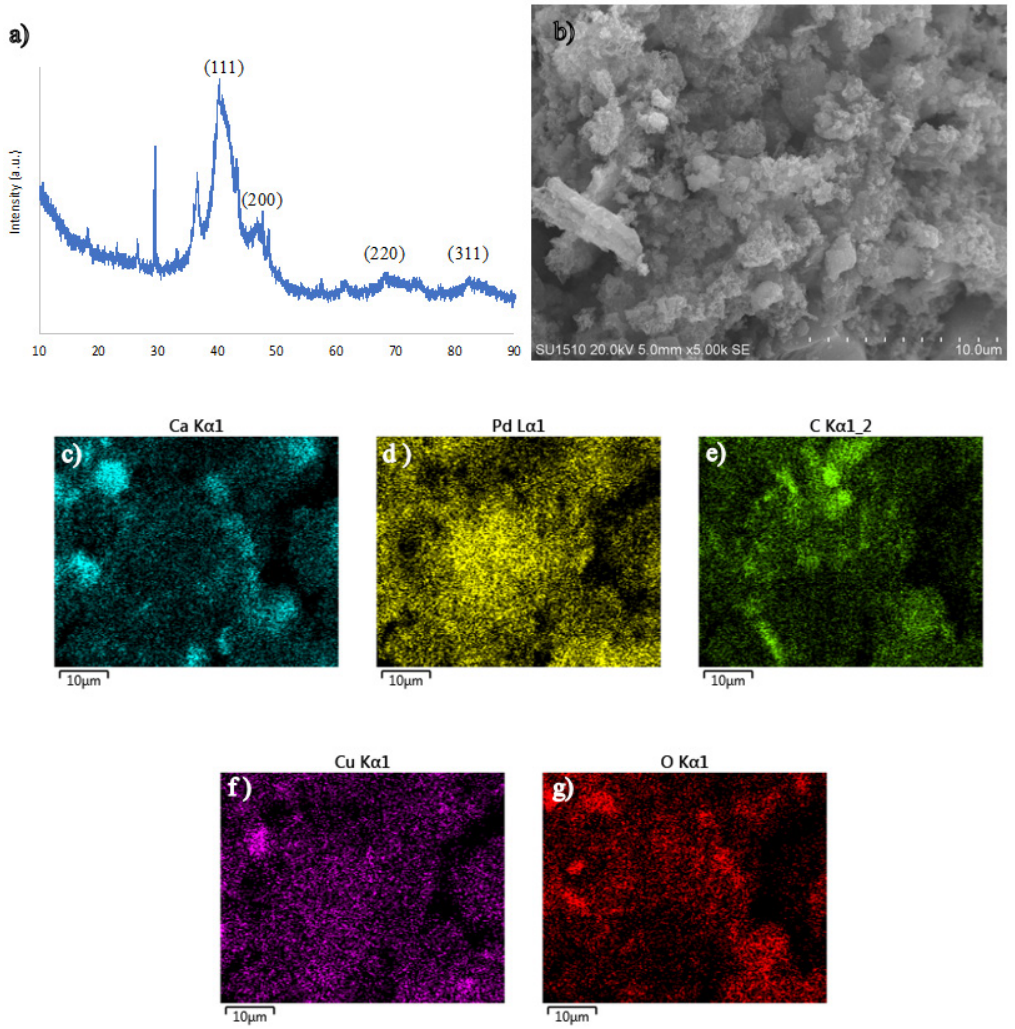


**Figure 2.** The XRD and SEM results of Pd/$SO_3$H/CNO.

of Pd (PdO), was observed in the structure, which was also confirmed by the XPS results. The XRD reflections observed at ca. 36.5°, 41.9°, 57.8°, and 60.3° correspond to the presence of the oxide form of Pd nanoparticles. The chemical analysis and the surface morphology of the samples were studied using SEM and EDS methods. The representative SEM image given in Fig. 2b indicates the three-dimensional surface morphology of the samples, which is essential for improved electrochemical activity and enlarged electrochemical active surface area. Furthermore, the elemental analysis results indicated that (Fig. 2c-g) suggested the homogeneous distribution of the Pd nanoparticles on the CNO surface. The presence of the S element, which originated from the sulfonate groups anchored on the CNO surface, was not observed from the EDS results, which may be attributed to the low S content on the CNO surface.

The surface chemistry of the Pd/$SO_3$H/CNO samples was studied using XPS analyses. The XPS results indicated O, C, Pd, S, and Cu elements on the sample surface (Fig. 3). As discussed earlier, the presence of Cu is attributed to the starting materials used to synthesize the CNO powder. Although the CNO samples were washed rigorously, residual Cu could not be removed from the sample. While EDS results did not show the S element on the CNO surface, the XPS results revealed the S element with 1.78 at. % ratio, confirming the successful modification of the CNO surface with $SO_3$H groups.

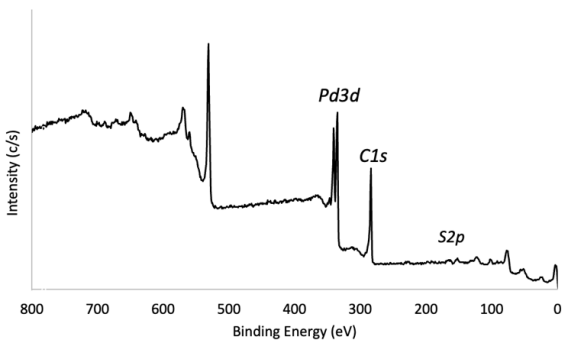


**Figure 3.** XPS survey of Pd/SO3H/CNO.

## Electrochemical behavior of the sensors

The CV voltammograms are shown in the with and without DA in 0.01 M PBS in Fig. 4a-c. While no oxidation peak was observed for the CNO and Pd/$SO_3$H/CNO in the DA-free electrolyte, upon the introduction of 100 µM DA into the solution, redox peaks appeared at 0.3 V and -0.2V. It is because of the two-electron oxidation of DA, yielding dopamine quinone [43]. Additionally, The oxidation current of Pd/$SO_3$H/CNO was much higher than that of CNO, indicating that Pd/$SO_3$H/CNO sample had much higher catalytic activity against the oxidation of DA. As shown in Fig. 4c, the unmodified CNO sample had a low analytical response. Note that Pd nanoparticles on the CNO surface enhances the electron mobility, improving the electrochemical activity. The EIS results of bare-GC, GC-CNO, and Pd/$SO_3$H-CNO-GC are given in Fig. 4d. The electron transfer resistance (Rct) of bare-GCE was found to be about 19 kΩ. The electron charge transfer resistance of the CNO and Pd/$SO_3$H/CNO modified GCs were found to be lower than bare-GC. However, Pd nanoparticles on the CNO surface improved the charge transfer rate, resulting in a lower semi-circle.

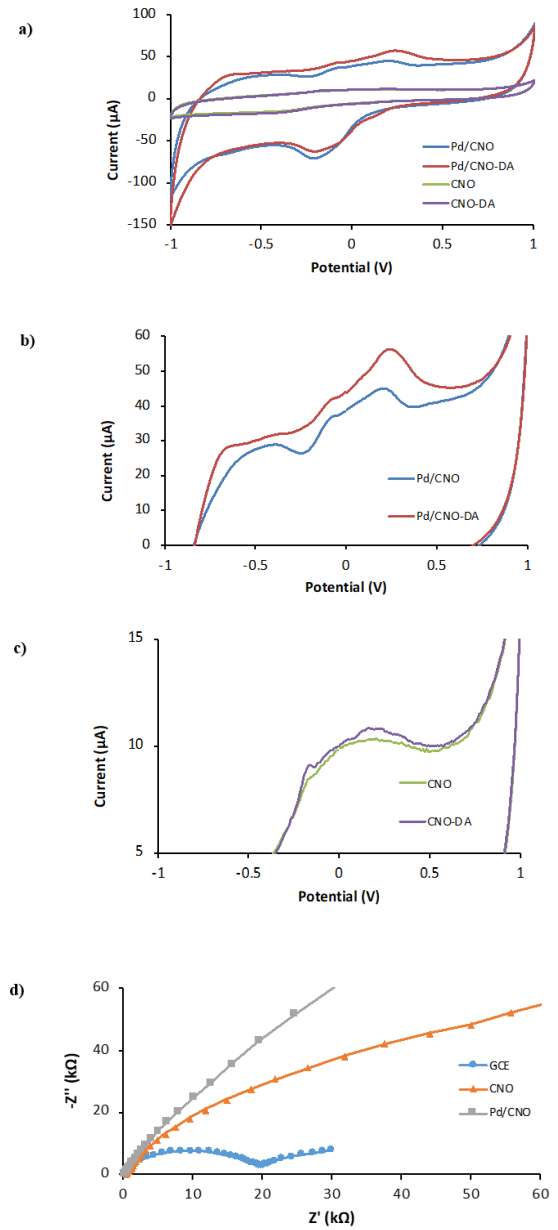


**Figure 4.** a) Electrochemical behavior of sensors in the presence of 100 µM DA, CV curves for b) Pd/CNO, c) CNO, and d) EIS diagrams.

The oxidation behavior of DA at various pH was evaluated using CV experiments and the results indicated that the electrolyte pH impacts the electrochemical activity towards DA. With the increase in the pH (Fig. 5a-b), the measured oxidation current decreased. The oxidation current decreased with the increasing pH of the solution. With the participation of protons in the DA oxidation, the peak potentials shifted to smaller values. According to the obtained CV curve, the highest current was obtained at the pH of 3.0. Therefore, further experiments were conducted at this pH value.

Fig. 5c shows the cyclic voltammograms recorded at different scan rates (10 to 400 mV/s) in the presence of 100 µM DA. The results showed that the oxidation current increased at higher scan rates. The relationship between the peak current and the scan rate graphs is shown in Figure 5d. The results show that DA oxidation on Pd/$SO_3$H/CNO is a surface-controlled reaction.

DPV measurement was performed between 10 µM and 400 µM of DA in 0.1 M PBS at a pH of 3.0 at a scan rate of 25 mV/s. (Fig. 6a). The oxidation peak appeared at 0.35 V for the sensor. The average linear regression plots and the concentration of DA results are shown in Fig. 6b. DA concentrations in the range of 100 µM to 400 µM (y=0.1355x+0.7833 and y= 0.0269x+10.959), with a $R^2$ value 0.9933 and 0.9993, respectively. The results suggested that the Pd modification of CNO enhances the electroactive sites and speed up the rate of electron transfer. Hence, Pd nanoparticles provide a high surface area to volume ratio and act as an effective performance to detect DA. These results showed that our sensor's upper linear range limit of 400 µM. The average sensitivity of the sensor was calculated to be 1.93 ± 0.14 µA $\mu M^{-1}$ $cm^{-2}$ from three different experiments (n=3, RSD %: 3.6). The detection limit (LOD) of the sensor was calculated according to the LOD=3s/S equation. The LOD of the sensor was found to be 2.44 µM (n=3). A low RSD % of 3.06 (n=3) was calculated from three different sensors, these results showed that this sensor has a high reproducibility of the fabrication process.

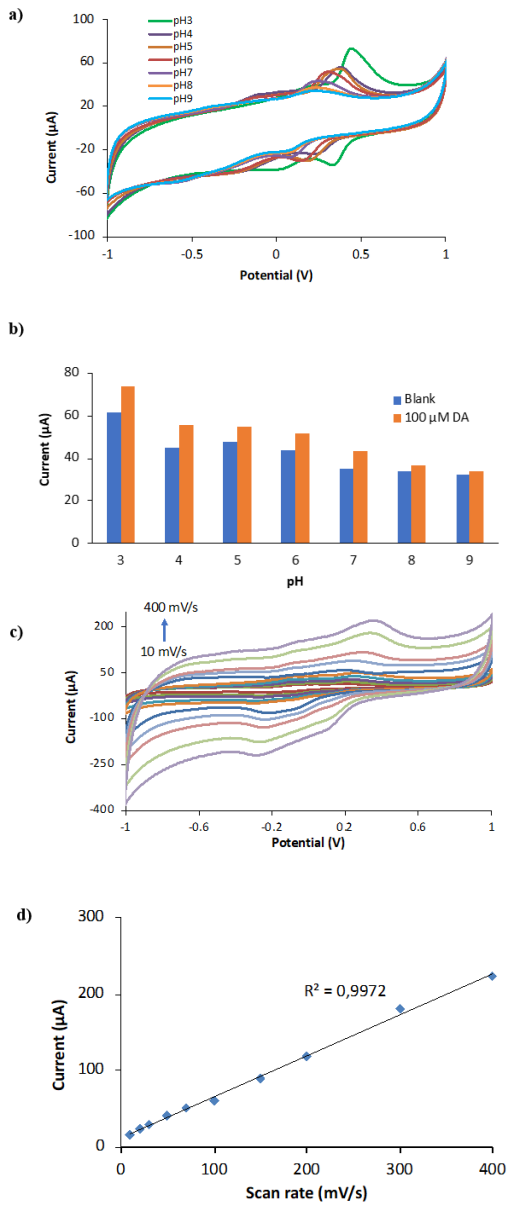


**Figure 5.** a) CV for 0.1 M PBS at different pH, b) the peak current at different pH, c) CV for different scan rates, d) Effect of scan rate on the peak current.

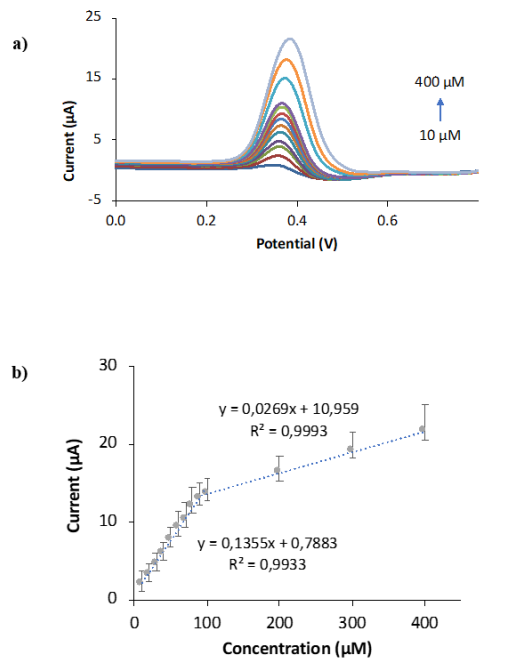


**Figure 6.** a) DPV results of the sensors at different concentrations of DA (10 µM to 400 µM), b) Linear plots versus concentration of DA and linear regression equations.

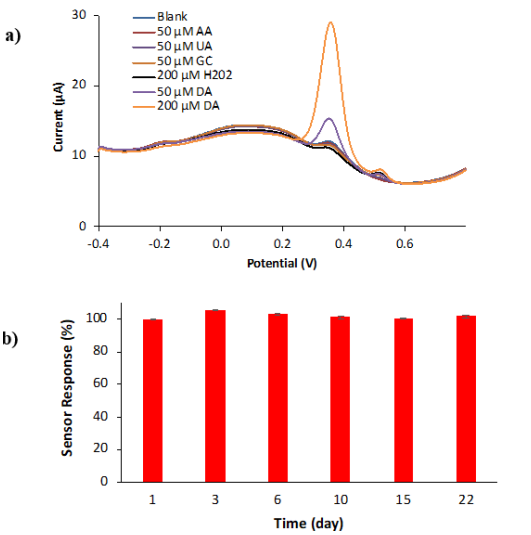


**Figure 7.** . a) Interference behavior in the detection of dopamine, b) Storage stability results of the sensor.

Note that the sensor can be used to detect DA in the linear range between 10 µM and 400 µM, which is wider than the previously published articles [37, 44] and even better than some of the Pd-based electrochemical sensors [45, 46]. The presence of different interferents can affect the sensor response in real samples therefore it is essential to evaluate the sensor response in terms of selectivity. Ascorbic acid (AA), uric acid (UA), glucose (GC), and hydrogen peroxide ($H_2O_2$) were used as the interferents. The selectivity study was conducted using DPV to evaluate the response of our sensors against the interferents. DPV measurements were recorded in the presence of 50 µM AA, UA, GC, and 200 µM $H_2O_2$ different DA concentrations of 50 and 200 µM (Fig. 7a). When the DA was added to the solution containing the interfering molecules, the current increased dramatically due to the detection of DA. Furthermore, no change in the peak current was obtained in the presence of interferents in the electrolyte, confirming a high selectivity. The storage stability of the sensors were studied by measuring the analytical response of the sensors against 20 µM DA for 22 days. The sensors were stored at room temperature throughout the stability experiments. The sensors yielded the analytical responses of 2.48 ± 0.28 (100 %) and 2.52 ± 0.57 µA (101.77 %) for the 1st and 22nd days, respectively. Fig. 7b shows that the sensor has a good sensor stability over time.

**Table 1.** Comparison of the performances of dopamine electrochemical sensor previously published reports.

| Electrode | Linear range (μM) | LOD (μM) | Ref |
|---|---|---|---|
| CNO/GRT SPE | 10–99.9 | 0.92 | [37] |
| Graphene-modified GC | 4-100 | 2.64 | [44] |
| RGOh/Pd-NPs | 1-150 | 0.233 | [45] |
| $Pd_3Pt_1$/PDDA-RGO | 4-200 | 0.04 | [46] |
| 3D SWNTs–Ppy composite | 5-50 | 5 | [47] |
| $NiFe_2O_4$-AC/GCE | 100-700 | 1 | [48] |
| Au-$Cu_2O$/rGO | 10-90 | 3.9 | [49] |
| Pd/$SO_3H$/CNO | 10-400 | 2.44 | This work |

SWNTs: single-wall carbon nanotubes; Ppy: polypyrrole
GC: Glass carbon
AC: Active carbon
CNO: Carbon nano-onion; GRT: Graphite
Pd3Pt1: Bimetallic nanoparticles Palladium and platinum
PDA: Polydopamine
PDDA: poly (diallyl dimethylammonium chloride)
RGO: Reduced graphene oxide

The electroanalytical performance of the Pd/SO3H/CNO-based electrochemical sensors was compared with published other reported DA sensor, as given in Table 1. The linear range of our sensors is much wider and the LOD of the sensor is much smaller than many previously published reports (Table 1). These results can be explained by the large surface area of Pd-doped CNO.

In order to assess the practical feasibility of the sensor, a commercial DA injection solution (Dopadren 200 mg/ml) was purchased from a local pharmacy. The dopamine injection solution was spiked into the PBS solution and DPV was carried out to determine the DA oxidation current. As seen in Table 2, the calculated recovery values were in the range of 97.76 % to 111.23 %. Each measurement was carried out three times (n=3). These results showed that the sensor had acceptable repeatability for the DA in real samples.

## CONCLUSION

In this study, the surface of CNO was modified with $SO_3H$ functional groups and Pd nanoparticles to achieve high electrochemical activity against DA. The electroanalytical performance analyses were conducted using CV and DPV techniques in PBS. The sensor yielded the highest response against DA at a pH 3.0. The LOD and linear range of the sensor were 2.44 μM, and 10–400 μM, respectively, and these data were compared with published reports. The TEM, XPS, and XRD results showed that $SO_3H$/CNO samples were decorated with Pd nanoparticles successfully. The Pd/$SO_3H$-CNO-modified GCs showed higher performance compared to CNO-modified GCs. The Pd/$SO_3H$/CNO-based sensors showed high electrochemical sensitivity, selectivity, and storage stability. Additionally, real sample analysis results indicated that our sensors can be used in real samples to detect DA.

**Table 2.** Real sample results of the sensor.

| Spiked (μM) | Calculated (μM) | Recovery (%) | RSD (%) |
|---|---|---|---|
| 10 | 10.09 | 100.90 | 10.0 |
| 20 | 22.24 | 111.23 | 1.0 |
| 30 | 29.32 | 97.76 | 5.48 |


## ACKNOWLEDGEMENT

The author acknowledges no financial support.


## CONFLICT OF INTEREST

The author states no conflict of interests.

## DATA AVAILABILITY

The dataset generated and/or analyzed in the current study is available from the corresponding author upon reasonable request.

## References


1. Zhao, K. and X. Quan, Carbon-Based Materials for Electrochemical Reduction of CO2 to C2+ Oxygenates: Recent Progress and Remaining Challenges. Acs Catalysis, 2021. 11(4): p. 2076-2097.
2. Karimi, A., et al., Graphene based enzymatic bioelectrodes and biofuel cells. Nanoscale, 2015. 7(16): p. 6909-6923.
3. Najafi, A.S.G. and T. Alizadeh, One-step hydrothermal synthesis of carbon nano onions anchored on graphene sheets for potential use in electrochemical energy storage. Journal of Materials Science: Materials in Electronics, 2022. 33(10): p. 7444-7462.
4. Pallavolu, M.R., et al., A novel hybridized needle-like Co3O4/N-CNO composite for superior energy storage asymmetric supercapacitors. Journal of Alloys and Compounds, 2022. 908: p. 164447.
5. Dalal, C., et al., Fluorescent carbon nano-onion as bioimaging probe. ACS Applied Bio Materials, 2021. 4(1): p. 252-266.
6. Kan, X., et al., 2008. - 112(- 13): p. - 4854.
7. Yeon, J.H., et al., Generation of carbon nano-onions by laser irradiation of gaseous hydrocarbons for high durability catalyst support in proton exchange membrane fuel cells. Journal of Industrial and Engineering Chemistry, 2019. 80: p. 65-73.
8. Camisasca, A. and S. Giordani, Carbon nano-onions in biomedical applications: Promising theranostic agents. Inorganica Chimica Acta, 2017. 468: p. 67-76.
9. Sharma, A., et al., 2022. - 7(- 42): p. - 37756.
10. Tripathi, K.M., et al., From the traditional way of pyrolysis to tunable photoluminescent water soluble carbon nano-onions for cell imaging and selective sensing of glucose. RSC advances, 2016. 6(44): p. 37319-37329.
11. Breczko, J., M.E. Plonska-Brzezinska, and L. Echegoyen, 2012. - 72: p. - 67.
12. Yang, J., Y. Zhang, and D.Y. Kim, Electrochemical sensing

performance of nanodiamond-derived carbon nano-onions: Comparison with multiwalled carbon nanotubes, graphite nanoflakes, and glassy carbon. Carbon, 2016. 98: p. 74-82.
13. Babar, D.G., et al., Carbon Nano Onions–Polystyrene Composite for Sensing S-Containing Amino Acids. Journal of Composites Science, 2020. 4(3): p. 90.
14. Sok, V. and A. Fragoso, Carbon nano-onion peroxidase composite biosensor for electrochemical detection of 2, 4-D and 2, 4, 5-T. Applied Sciences, 2021. 11(15): p. 6889.
15. Aparicio-Martínez, E., et al., Flexible electrochemical sensor based on laser scribed Graphene/Ag nanoparticles for non-enzymatic hydrogen peroxide detection. Sensors and Actuators B: Chemical, 2019. 301: p. 127101.
16. Ipekci, H.H., et al., Ink-jet Printing of Particle-Free Silver Inks on Fabrics with a Superhydrophobic Protection Layer for Fabrication of Robust Electrochemical Sensors. Microchemical Journal, 2021: p. 106038.
17. Mohapatra, J., et al., Enzymatic and non-enzymatic electrochemical glucose sensor based on carbon nano-onions. Applied Surface Science, 2018. 442: p. 332-341.
18. Uzunoglu, A., A.D. Scherbarth, and L. Stanciu, Bimetallic PdCu/SPCE non-enzymatic hydrogen peroxide sensors. 2015: Sensors and Actuators B: Chemical. p. 968-976.
19. Uzunoglu, A. and H.H. Ipekci, The use of CeO2-modified Pt/C catalyst inks for the construction of high-performance enzyme-free H2O2 sensors. Journal of Electroanalytical Chemistry, 2019. 848: p. 113302.
20. Wang, J., et al., Dopamine and uric acid electrochemical sensor based on a glassy carbon electrode modified with cubic Pd and reduced graphene oxide nanocomposite. Journal of colloid and interface science, 2017. 497: p. 172-180.
21. Uzunoglu, A., et al., PdAg-decorated three-dimensional reduced graphene oxide-multi-walled carbon nanotube hierarchical nanostructures for high-performance hydrogen peroxide sensing. Mrs Communications, 2018. 8(3): p. 680-686.
22. Sohouli, E., et al., Introducing a novel nanocomposite consisting of nitrogen-doped carbon nano-onions and gold nanoparticles for the electrochemical sensor to measure acetaminophen. Journal of Electroanalytical Chemistry, 2020. 871: p. 114309.
23. Dar, R.A., et al., Performance of palladium nanoparticle–graphene composite as an efficient electrode material for electrochemical double layer capacitors. Electrochimica Acta, 2016. 196: p. 547-557.
24. Klębowski, B., et al., Applications of noble metal-based nanoparticles in medicine. International journal of molecular sciences, 2018. 19(12): p. 4031.
25. Agostini, G., et al., Effect of pre-reduction on the properties and the catalytic activity of Pd/carbon catalysts: A comparison with Pd/Al2O3. ACS Catalysis, 2014. 4(1): p. 187-194.
26. Fu, L., et al., Advanced Catalytic and Electrocatalytic Performances of Polydopamine-Functionalized Reduced Graphene Oxide-Palladium Nanocomposites. ChemCatChem, 2016. 8(18): p. 2975-2980.
27. Law, C.K.Y., et al., Electrochemically assisted production of biogenic palladium nanoparticles for the catalytic removal of micropollutants in wastewater treatment plants effluent. Journal of Environmental Sciences, 2022.
28. T, K., et al., - O5.1. Striatal Dopamine and Reduced Reward Prediction Error Signaling In. - Schizophr Bull. 2020 May;46(Suppl 1):S11. doi: 10.1093/schbul/sbaa028.024. Epub, (- 0586-7614 (Print)): p. T - ppublish.
29. Whitton, A.E., et al., Baseline reward processing and ventrostriatal dopamine function are associated with pramipexole response in depression. Brain, 2020. 143(2): p. 701-710.
30. Napier, T.C., A. Kirby, and A.L. Persons, 2020. - 102.
31. Pan, X., et al., Dopamine and Dopamine Receptors in Alzheimer's Disease: A Systematic Review and Network Meta-Analysis. Frontiers in Aging Neuroscience, 2019. 11.
32. Feng, P., et al., 2018. - 10(- 5): p. - 4368.
33. Lin, T.-Y., et al., Diagnosis by simplicity: an aptachip for dopamine capture and accurate detection with a dual colorimetric and fluorometric system. Journal of Materials Chemistry B, 2018. 6(20): p. 3387-3394.
34. Zhang, X., et al., A simple, fast and low-cost turn-on fluorescence method for dopamine detection using in situ reaction. Analytica chimica acta, 2016. 944: p. 51-56.
35. Vuorensola, K., H. Sirén, and U. Karjalainen, Determination of dopamine and methoxycatecholamines in patient urine by liquid chromatography with electrochemical detection and by capillary electrophoresis coupled with spectrophotometry and mass spectrometry. Journal of Chromatography B, 2003. 788(2): p. 277-289.
36. Uzunoglu, A. and L. Stanciu, Novel CeO2-CuO-decorated enzymatic lactate biosensors operating in low oxygen environments. Analytica Chimica Acta, 2016. 909: p. 121-128.
37. Cumba, L.R., et al., Electrochemical properties of screen-printed carbon nano-onion electrodes. Molecules, 2020. 25(17): p. 3884.
38. Ozoemena, O.C., et al., Electrochemical sensing of dopamine using onion-like carbons and their carbon nanofiber composites. Electrocatalysis, 2019. 10(4): p. 381-391.
39. Han, F.-D., B. Yao, and Y.-J. Bai, Preparation of carbon nano-onions and their application as anode materials for rechargeable lithium-ion batteries. The Journal of Physical Chemistry C, 2011. 115(18): p. 8923-8927.
40. Xin, L., et al., Polybenzimidazole (PBI) Functionalized Nanographene as Highly Stable Catalyst Support for Polymer Electrolyte Membrane Fuel Cells (PEMFCs). Journal of the Electrochemical Society, 2016. 163(10): p. F1228-F1236.
41. Xing, L., et al., Understanding Pt Nanoparticle Anchoring on Graphene Supports through Surface Functionalization. Acs Catalysis, 2016. 6(4): p. 2642-2653.
42. Bozkurt, S., et al., A hydrogen peroxide sensor based on TNM functionalized reduced graphene oxide grafted with highly monodisperse Pd nanoparticles. Analytica Chimica Acta, 2017. 989: p. 88-94.
43. Wu, D., et al., 2014. - 116: p. - 249.
44. Liu, Q., et al., Electrochemical detection of dopamine in the presence of ascorbic acid using PVP/graphene modified electrodes. Talanta, 2012. 97: p. 557-562.
45. Palanisamy, S., S. Ku, and S.-M. Chen, Dopamine sensor based on a glassy carbon electrode modified with a reduced graphene oxide and palladium nanoparticles composite. Microchimica Acta, 2013. 180(11): p. 1037-1042.
46. Yan, J., et al., Simultaneous electrochemical detection of ascorbic acid, dopamine and uric acid based on graphene anchored with Pd–Pt nanoparticles. Colloids and Surfaces B: Biointerfaces, 2013. 111: p. 392-397.
47. Min, K. and Y.J. Yoo, Amperometric detection of dopamine based on tyrosinase–SWNTs–Ppy composite electrode. Talanta, 2009. 80(2): p. 1007-1011.
48. Aparna, T. and R. Sivasubramanian, Selective electrochemical detection of dopamine in presence of ascorbic acid and uric acid using NiFe2O4-activated carbon nanocomposite modified glassy carbon electrode. Materials Today: Proceedings, 2018. 5(8): p. 16111-16117.

49. Aparna, T., R. Sivasubramanian, and M.A. Dar, One-pot synthesis of Au-Cu2O/rGO nanocomposite based electrochemical sensor for selective and simultaneous detection of dopamine and uric acid. Journal of Alloys and Compounds, 2018. 741: p. 1130-1141.